

The Impact of Spin–Orbit Interaction on the Image States of High-Z Materials

Jürgen Braun* and Hubert Ebert

Due to many important technical developments over the past two decades angle-resolved (inverse) photoemission has become the method of choice to study experimentally the bulk and surface-related electronic states of solids in the most detailed way. Due to new powerful photon sources as well as efficient analyzers and detectors extremely high energy and angle resolution are achieved nowadays for spin-integrated and also for spin-resolved measurements. These developments allow in particular to explore the influence of spin–orbit coupling on image potential states of simple metals like Ir, Pt, or Au with a high atomic number as well as new types of materials as for example topological insulators. Herein, fully relativistic angle- and spin-resolved inverse photoemission calculations are presented that make use of the spin-density matrix formulation of the one-step model. This way a quantitative analysis of all occupied and unoccupied electronic features in the vicinity of the Fermi level is achieved for a wide range of excitation energies. Using this approach, in addition, it is possible to deal with arbitrarily ordered but also disordered systems. Because of these features, the one-step or spectral function approach to photoemission permits detailed theoretical studies on a large variety of interesting solid-state systems.

understanding of the special spin topology is of great interest in the scientific community. Prototypical examples for such TI systems are Bi₂Se₃, Bi₂Te₃, or Sb₂Te₃ but also slightly more complex compounds as for example Bi₂Te₂Se. In contrast to ordinary insulators and semiconductors, the bulk and surface-related electronic features are coupled in TI materials on a topological level. This means that a nontrivial topological entanglement between the bulk electronic structure and corresponding surface-related electronic states triggers the existence of a topological surface state (TSS). Therefore the appearance of a TSS is intimately connected with the bulk electronic properties. This is in contrast to conventional surface features, as, for example, bulk-derived surface states or resonances which are triggered by the geometric surface properties, where the surface potential itself plays an important role.

With this contribution we investigate the impact of the spin–orbit interaction on the so-called image potential states of a prototypical TI system and compare our spectroscopical results with the corresponding intensity pattern and spin polarizations calculated for three simple metal systems.

1. Introduction

3D topological insulators (TIs) are new and promising candidates for various technological applications. These new types of solid phases are typically characterized by an insulating bulk electronic structure in combination with highly polarized metallic surface states.^[1–5] Spin and momentum locking and protection by time-reversal symmetry which are present in TI systems qualify these solid phases as prominent materials in the field of spintronics.^[6–23] This way a quantitative


2. Theoretical and Computational Details

In our theoretical investigation we use the relativistic one-step model of photoemission, in its spin-density matrix formulation. This guarantees for a quantitative description of all three components of the spin polarization vector of the photocurrent.^[24–26] Within the spin-density matrix approach the photocurrent is completely represented by the following 2×2 matrix:^[27]

$$\bar{\rho}_{ss'}(\mathbf{k}_{\parallel}, \epsilon_f) = \langle s, \epsilon_f, \mathbf{k}_{\parallel} | G_f^A \Delta G_i^R \Delta^\dagger G_f^R | \epsilon_f, \mathbf{k}_{\parallel}, s' \rangle \quad (1)$$

Here ϵ_f defines the single-particle energy of the outgoing photoelectron, \mathbf{k}_{\parallel} defines the wavevector component parallel to the surface, and the variable s denotes the corresponding spin character, whereas Δ denotes the dipole operator. The retarded (R) and advanced (A) single-particle propagators $G_f^{R,(A)}$ for the final state and the retarded propagator G_i^R for the initial state are numerically obtained by use of standard-layer Korringa–Kohn–Rostoker (LKKR) multiple scattering techniques.^[28] In the relativistic case both propagators are represented by

Prof. J. Braun, Prof. H. Ebert
Department Chemie
Ludwig-Maximilians-Universität München
Butenandtstr. 5–11, München 81377, Germany
E-mail: juergen.braun@cup.uni-muenchen.de

 The ORCID identification number(s) for the author(s) of this article can be found under <https://doi.org/10.1002/pssb.202000026>.

© 2020 The Authors. Published by WILEY-VCH Verlag GmbH & Co. KGaA, Weinheim. This is an open access article under the terms of the Creative Commons Attribution-NonCommercial-NoDerivs License, which permits use and distribution in any medium, provided the original work is properly cited, the use is non-commercial and no modifications or adaptations are made.

DOI: 10.1002/pssb.202000026

4×4 matrices. In Equation (1) the final state is represented by a time-reversed (spin-polarized) low energy electron diffraction [(SP)LEED] state $G_f^R|\epsilon_f, \mathbf{k}_\parallel, s\rangle$. This implies that the photocurrent does not reflect the intrinsic variables, but the single-particle energy ϵ_f of the outgoing photoelectron, the corresponding wave vector \mathbf{k}_\parallel component parallel to the surface, and its spin character s . From Equation (1) the spin-density matrix ρ follows as

$$\rho_{ss'}(\mathbf{k}_\parallel, \epsilon_f) = \frac{1}{2i}(\tilde{\rho}_{ss'}(\mathbf{k}_\parallel, \epsilon_f) - \tilde{\rho}_{s's}^*(\mathbf{k}_\parallel, \epsilon_f)) \quad (2)$$

This way, the intensity of the photocurrent results in

$$I(\mathbf{k}_\parallel, \epsilon_f) = \text{Tr}(\rho_{ss'}(\mathbf{k}_\parallel, \epsilon_f)) \quad (3)$$

with the corresponding spin polarization vector given by

$$P = \frac{1}{I} \text{Tr}(\sigma \rho) \quad (4)$$

Finally, the spin-projected photocurrent is obtained from the following expression

$$I_n^\pm = \frac{1}{2}(1 \pm \mathbf{n} \cdot \mathbf{P}) \quad (5)$$

with the spin polarization (\pm) referring to vector \mathbf{n} . This way, one is able to compute all three components of the spin polarization vector \mathbf{P} .^[26]

To calculate the complete spin polarization vector \mathbf{P} within the one-step model of photoemission, all four elements of the spin-density matrix must be computed, where special care has to be taken when dealing with the final state. The final state which is given by a time-reversed (SP)LEED state is computed first applying unpolarized boundary conditions, which means that the final state at the detector is determined by the corresponding average $\chi = (1, 1)/\sqrt{2}$ of the two basis spinors $\chi = (1, 0)/\sqrt{2}$ and $\chi = (0, 1)/\sqrt{2}$. In a second step, by use of the plane-wave representation of the final state, one can extract the spin-up $|\epsilon_f, \mathbf{k}_\parallel, \uparrow\rangle$ and spin-down components $|\epsilon_f, \mathbf{k}_\parallel, \downarrow\rangle$ of the time-reversed (SP)LEED state. Inserting then proper combinations of the two spin components of the final state in Equation (1) all four elements of the spin-density matrix can be calculated by four separate calculations.

Within a plain LDA calculation it is not possible to describe quantitatively the correct long range behavior of the surface potential $V(z)$.^[26] The solution for this problem is the use of a modified electronic potential in the spectroscopical analysis that consists of a self-consistently calculated bulk or layer-dependent crystal potential for a semi-infinite stack of atomic layers plus a model potential as for example of Rundgren Malmström type. With this procedure a quantitative description of the complete system is guaranteed in the spectroscopical analysis. This includes all matrix element effects as well as initial and final state effects even in the barrier potential region. The coefficients which define the final and initial state wave fields can be formulated in terms of the bulk reflection and surface potential scattering matrices^[26,29] and account for all symmetry properties of a Rashba split surface state.

A realistic description of the surface barrier is given in the paramagnetic case through a spin-independent Rundgren–Malmström potential,^[30] which represents a 1D z -dependent

function $V_B(z)$ with the z -axis directed perpendicular to the surface pointing into the semi-infinite bulk. The potential $V_B(z)$ connects the asymptotic regime ($V_B(z) \propto 1/z$, $z_A > z$) to the bulk muffin-tin zero V_{or} by a third-order polynomial $P(z)$, e.g., defining a polynomial range $z_E > z > z_A$. The second parameter z_E defines the point where the surface region ends and the bulk region starts. The third parameter z_1 ($z_E > z_1 > z_A$), which allows to modify the shape of the potential function, is typically interpreted in terms of the classical image plane.^[30]

As special care is taken on the surface-barrier-induced image states (IS), it remains to be illustrated in more detail the corresponding computational scheme which results in the surface contribution of the total photoemission intensity. The following set of equations represents the final state wavefunction in the surface region. By means of the following contribution $\tilde{\rho}_{ss'}^{\text{SUR}}(\epsilon_f, \mathbf{k}_\parallel)$ one takes care of the surface:

$$\tilde{\rho}_{ss'}^{\text{SUR}}(\epsilon_f, \mathbf{k}_\parallel) = \int d^3r \Psi_{2s}^*(\mathbf{r}) \Delta \Phi_{1s'}(\mathbf{r}) \quad (6)$$

with

$$\Phi_{1s'}(\mathbf{r}) = \int d^3r' G_{1,\text{SUR}}^+(\mathbf{r}, \mathbf{r}') \Delta^* \Psi_{2s'}(\mathbf{r}') \quad (7)$$

For a z -dependent barrier potential $V_B = V_B(z)$, the initial and final state wavefields must be computed in the region of the surface barrier. Both wavefields $\Phi_{1s'}(\mathbf{r})$ and $\Psi_{2s}(\mathbf{r})$ can be decomposed into z -dependent and corresponding parallel components

$$\Phi_{1s'}(\mathbf{r}) = \sum_{\mathbf{g}} \phi_{1\mathbf{g}'}(z) e^{i\mathbf{k}_{\parallel\mathbf{g}}(\mathbf{r}-\mathbf{c}_1)} \quad (8)$$

$$\Psi_{2s}(\mathbf{r}) = \sum_{\mathbf{g}} \psi_{2\mathbf{g}s}(z) e^{i\mathbf{k}_{2\mathbf{g}}(\mathbf{r}-\mathbf{c}_1)} \quad (9)$$

with the regular solutions of the Schrödinger equation $\phi_{1\mathbf{g}}$ and $\psi_{2\mathbf{g}}$ to the reciprocal lattice vector \mathbf{g} for $V_B(z)$ in the range $c_{1z} > z > -\infty$. $G_{1,\text{SUR}}^+$ denotes the surface part of the corresponding retarded Green function. Δ denotes the dipole operator. The value $c_{1z} = z_E$ defines the point, where the surface potential joins smoothly to the inner potential of the bulk crystal.

The explicit computation of the surface barrier contribution results in

$$\tilde{\rho}_{ss'}^{\text{SUR}}(\epsilon_f, \mathbf{k}_\parallel) = \frac{A_z}{2\omega c} e^{i\mathbf{q}_\parallel \cdot \mathbf{c}_1} \sum_{\mathbf{g}} \int_{-\infty}^{c_{1z}} dz \psi_{2\mathbf{g}s}(z) \frac{dV_B}{dz} \phi_{1s'\mathbf{g}}(z) e^{i\mathbf{q}_z z} \quad (10)$$

where again A_z denotes the z -component of the photon field amplitude \mathbf{A}_0 , and \mathbf{q} denotes the corresponding wavevector. The photon frequency is given by ω and c denotes the speed of light.

The self-consistent electronic structure calculations for the three metal surfaces and for Bi_2Se_3 were carried out within the ab initio framework of density functional theory. The Vosko, Wilk, and Nusair parameterization for the exchange and correlation potential was used.^[31] The electronic structure of all four systems was calculated in a fully relativistic mode by solving the corresponding Dirac equation. In detail the relativistic multiple scattering or KKR formalism in the TB-KKR mode^[32] was applied in the numerical procedure. The resulting

half-space electronic structure represented by single-site scattering matrices for different layers and the corresponding wave functions for initial- and final-state energies were used as input quantities for the corresponding spectroscopic analysis. For this calculation, in addition, we took into account the Rundgren-type surface barrier.^[30] Furthermore we took care of impurity scattering, via a small constant imaginary value of $V_i = 0.03$ eV that was used for the initial state in all cases. For the final state a constant imaginary value of $V_f = 1.8$ eV has been chosen again in a phenomenological way for an excitation energy of about 10 eV that we used in our photoemission calculations.

3. Ir(111), Pt(111), and Au(100)

A variety of experimental as well as theoretical photoemission studies have been conducted within the past decades on Ir, Pt, and Au^[29,33–44] with linear and circular polarized light. Most of these studies were focused on the bulk electronic structure and on bulk-derived surface states. The image potential states and especially the impact of spin–orbit interaction on these electronic features are investigated only recently in two experimental studies,^[45,46] on Au(100) and on graphene-covered Ir(111) but with controversial results. We show here in **Figure 1** our calculational results for Ir(111) obtained for a photon energy of 9.9 eV with p-polarized light. We used for the work function of the clean Ir(111) surface the value $\phi_{\text{Ir}} = 5.8$ eV.^[47] With the optimized surface barrier parameters that we used in our analysis the energetics and dispersion of the well-known Ir(111) surface resonance^[43] could be quantitatively reproduced. The energetic position of the first IS for $k_{\parallel} = 0$ has been found to be $E = 0.535$ eV below E_{vac} . This value is in very good agreement with the corresponding experimental value found for the graphene-covered Ir(111) surface. Tognolini et al. obtained $E = 0.55$ eV

below E_{vac} , where the measured value for the work function was $\phi_{\text{Ir}} = 4.45 \pm 0.05$ eV.^[45] The left panel of **Figure 1** shows the intensity pattern and in the right panel the corresponding Rashba component of the spin polarization is shown. In comparison with the experimental findings in previous studies^[45,46] the splitting is very small with a value $\Delta k = 0.004 \text{ \AA}^{-1}$. The corresponding Rashba parameter results in $\alpha_R = 0.005 \text{ eV \AA}$. This means that the Rashba splitting of the first IS on Ir(111) is smaller by a factor of 7 compared to the Rashba splitting of the Au(111) Shockley surface state^[48] and this way at the border of the experimental resolution. Inspecting the right panel in **Figure 1** the spin polarization shows the typical Rashba behavior with an asymmetric sign change of the corresponding polarization component.

For Pt(111) the situation appears very similar. We used for the work function of the clean Pt(111) surface the value $\phi_{\text{Pt}} = 6.1$ eV.^[47] For the surface barrier we used the same parameterization as in a previous study.^[49] The energetic position for the first IS at $k_{\parallel} = 0$ on Pt(111) has been found to be $E = 0.558$ eV below E_{vac} . This value is also in good agreement with the corresponding experimental value of $E = 0.539 \pm 0.03$ eV.^[50] The corresponding intensity pattern is presented in the left panel and the spin polarization again in the right panel of **Figure 2**. In contrast to Ir(111) the splitting is slightly larger with a value $\Delta k = 0.0045 \text{ \AA}^{-1}$ and a Rashba parameter $\alpha_R = 0.0052 \text{ eV \AA}$. These results seem reasonable as the atomic number is slightly higher. This splitting remains about six times smaller compared with the Rashba splitting of the *sp*-derived Shockley state of Pt(111).^[49]

As a third example we have calculated the dispersion relation of the first IS on Au(100). We used for the work function of the clean Au(100) surface the value $\phi_{\text{Au}} = 5.47$ eV.^[51] The barrier parameters were optimized to be able to reproduce the experimental and theoretical energetics of the corresponding surface features dispersed on Au(100).^[51,52] Explicitly, the first IS on Au(100) has been found to be at $E = 0.69$ eV below E_{vac} from

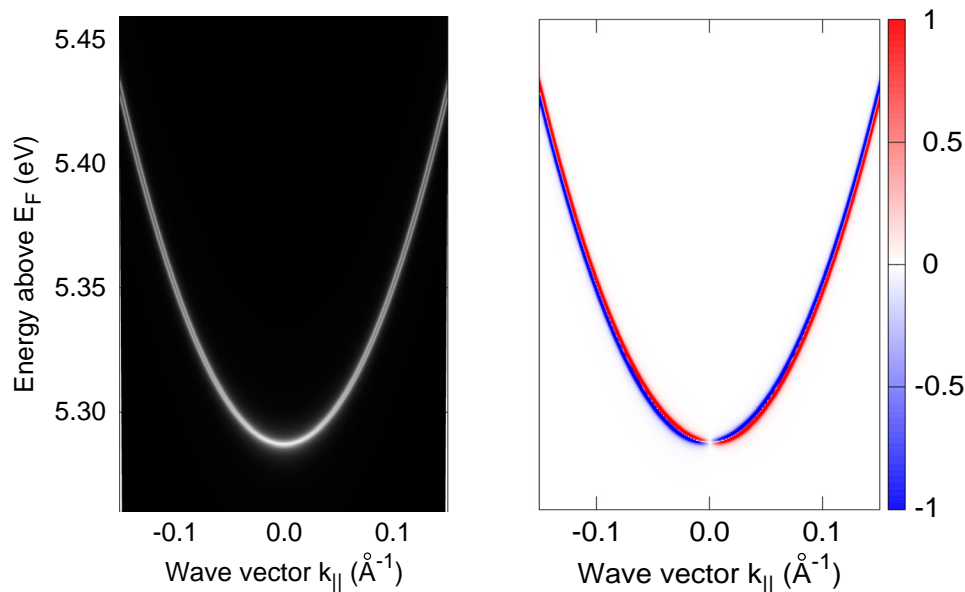


Figure 1. Dispersion of the first IS on Ir(111). Intensity (left panel) and Rashba component of the spin polarization (right panel) calculated for a photon energy of 9.9 eV along $\bar{\Gamma} - \bar{K}$ with p-polarized light. The Rashba splitting counts to $\Delta k = 0.004 \text{ \AA}^{-1}$.

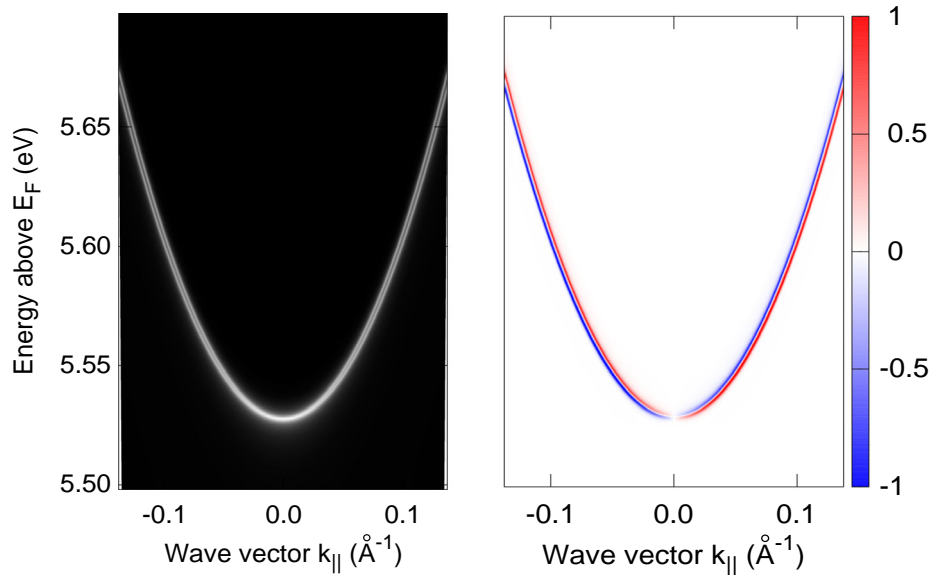


Figure 2. Dispersion of the first IS on Pt(111). Intensity (left panel) and Rashba component of the spin polarization (right panel) calculated for a photon energy of 9.9 eV along $\bar{\Gamma} - \bar{K}$ with p-polarized light. The Rashba splitting counts to 0.0045 \AA^{-1} .

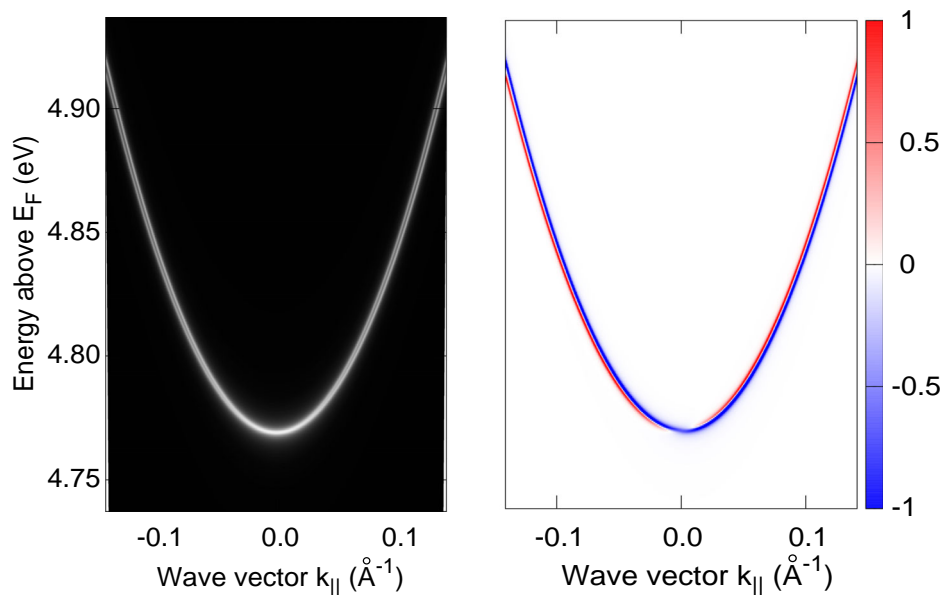


Figure 3. Dispersion of the first IS on Au(100). Intensity (left panel) and Rashba component of the spin polarization (right panel) calculated for a photon energy of 9.9 eV along $\bar{\Gamma} - \bar{X}$ with p-polarized light. The Rashba splitting counts to $\Delta k = 0.0047 \text{ \AA}^{-1}$.

our calculations. The theoretical result is shown in **Figure 3**, again with the dispersion of the IS presented in the left panel and the spin polarization shown in the right panel. Astonishingly the splitting is not significantly increased in comparison with the Pt case. It follows quantitatively that $\Delta k = 0.0047 \text{ \AA}^{-1}$ and $\alpha_R = 0.0054 \text{ eV \AA}$. This means that the slight increase in the atomic number is not sufficient to create a splitting even for IS on Au measurable with modern experimental apparatus. This of course excludes the three prototypical paramagnetic metals Ir, Pt, and Au as candidates which would allow for an experimental verification of the spin-orbit split IS.

If one inspects the periodic table, Bi metal or even more sophisticated materials containing Bi seem a better choice. We decided to inspect the prototypical TI system Bi_2Se_3 , aiming on a Rashba splitting of the IS that could be measured in photoemission experiments.

4. Bi_2Se_3

A quantitative determination of the spin texture of the unoccupied band regime in TI systems like Bi_2Se_3 is possible, as

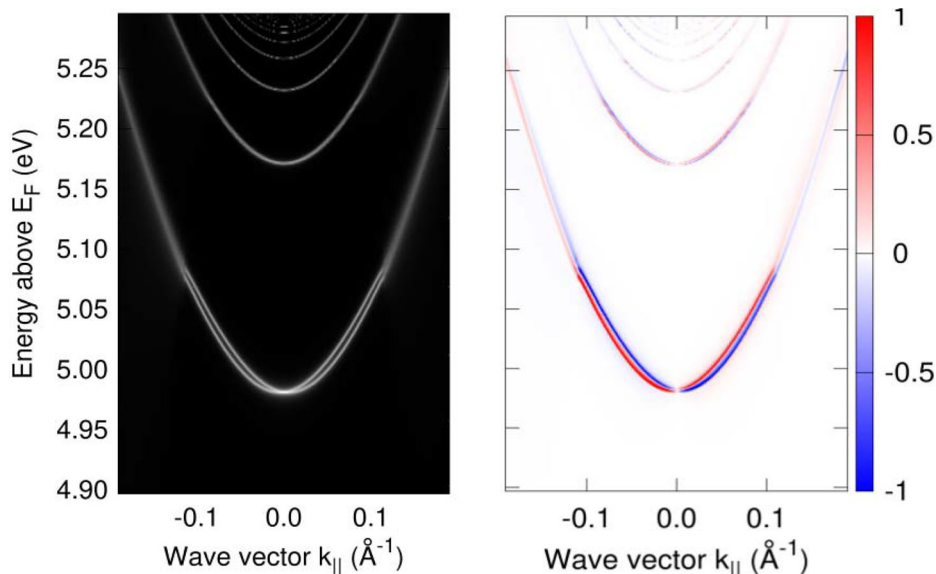


Figure 4. Dispersion of the series of IS on Bi₂Se₃(0001). Intensity (left panel) and Rashba component of the spin polarization (right panel) calculated for a photon energy of 9.9 eV along $\bar{\Gamma} - \bar{K}$ with p-polarized light. The Rashba splitting counts to $\Delta k = 0.0065 \text{ \AA}^{-1}$.

demonstrated in a joint experimental and theoretical study, where spin- and angle-resolved inverse photoemission (IPE) data were compared with calculations for both the intrinsic band structure and, within, the one-step model of (inverse) photoemission, the expected IPE spectral intensities.^[23] This study allowed to unravel the intrinsic dispersion as well as the spin texture of all unoccupied bulk states and bulk-derived surface bands. In detail it was found that spin–orbit coupling in the initial-state wave functions plays an important role and this way revealed that spin-dependent effects in the final state considerably influence the photoelectron spin polarization.

For the work function of the clean Bi₂Se₃(0001) surface we used the value $\phi_{\text{Bi}_2\text{Se}_3} = 5.35 \text{ eV}$ and the parameterization which was successfully used in a previous study.^[23] The resulting first IS on Bi₂Se₃(0001) appears at an energy $E = 0.64 \text{ eV}$ below E_{Vac} . The calculational result is shown in **Figure 4** where we present our IPE analysis for the series of images states on Bi₂Se₃(0001). It is clearly observable that a significant influence of spin–orbit coupling is present in the dispersion of the different IS and in consequence on the Rashba component of spin polarization. In fact the splitting of the first IS is two times larger as the Rashba splitting in Ir, Pt, or Au. The corresponding parameters result in $\Delta k = 0.0065 \text{ \AA}^{-1}$ and $\alpha_R = 0.011 \text{ eV \AA}$. Inspecting the dispersion behavior in the left panel of Figure 4, one can observe that even in the second IS a significant splitting occurs. This is also observable from the Rashba component of the spin polarization which is shown in the right panel of Figure 4. The values obtained for Δk and α are slightly larger than the corresponding ones measured for the Shockley state on Cu(111)^[53–55] where a value $\Delta k = 0.006 \text{ \AA}^{-1}$ was found. This means that our theoretical prediction for the Rashba splitting of the first IS on Bi₂Se₃(0001) can be experimentally verified by state-of-the-art photoemission measurements. As a conclusion from our spectroscopical analysis it turns out that metals or compounds containing elements with atomic numbers definitely higher than

$Z = 80$ exhibit pronounced spin–orbit effects even in the image potential states.

5. Conclusions

The impact of spin–orbit interaction on barrier-induced surface states appearing on Ir(111), Pt(111), Au(100), and Bi₂Se₃(0001) has been studied. We found that Rashba-type splitting exists in all four cases where on the three metal surfaces the splitting seems to be too small for an experimental verification at the moment. For Bi₂Se₃(0001) the situation is different as Rashba splitting is significantly larger and should be measurable by state-of-the-art spin-resolved photoemission experiments as the corresponding Rashba parameter is comparable with that of the Shockley surface state on Cu(111). In conclusion, the one-step model of photoemission in its spin-density matrix formulation allows to unravel the Rashba-type spin texture of IS located in front of simple metal surfaces as well as more sophisticated TI systems.

Acknowledgements

The authors gratefully acknowledge financial support by the Deutsche Forschungsgemeinschaft within the priority program SPP1666 (project EB 154/26). The authors also thank Oliver Rader and Jaime Sánchez-Barriga for their fruitful collaboration. Open access funding enabled and organized by Projekt DEAL.

Conflict of Interest

The authors declare no conflict of interest.

Keywords

image states, photoemission, spin–orbit interaction

Received: January 14, 2020
Revised: June 5, 2020
Published online: July 23, 2020

- [1] C. L. Kane, E. J. Mele, *Phys. Rev. Lett.* **2005**, *95*, 226801.
- [2] Y. L. Chen, J. G. Analytis, J. H. Chu, Z. K. Liu, S. K. Mo, X. L. Qi, H. J. Zhang, D. H. Lu, X. Dai, Z. Fang, S. C. Zhang, I. R. Fisher, Z. Hussain, Z. X. Shen, *Science* **2009**, *325*, 178.
- [3] M. Z. Hasan, C. L. Kane, *Rev. Mod. Phys.* **2010**, *82*, 3045.
- [4] D. Hsieh, Y. Xia, D. Qian, L. Wray, J. H. Dil, F. Meier, J. Osterwalder, L. Patthey, J. G. Checkelsky, N. P. Ong, A. V. Fedorov, H. Lin, A. Bansil, D. Grauer, Y. S. Hor, R. J. Cava, M. Z. Hasan, *Nature* **2009**, *460*, 1101.
- [5] M. R. Scholz, J. Sánchez-Barriga, D. Marchenko, A. Varykhalov, A. Volykhov, L. V. Yashina, O. Rader, *Phys. Rev. Lett.* **2012**, *108*, 256810.
- [6] H. Mirhosseini, J. Henk, *Phys. Rev. Lett.* **2012**, *109*, 036803.
- [7] M. R. Scholz, J. Sánchez-Barriga, J. Braun, D. Marchenko, A. Varykhalov, M. Lindroos, Y. J. Wang, H. Lin, A. Bansil, J. Minár, H. Ebert, A. Volykhov, L. V. Yashina, O. Rader, *Phys. Rev. Lett.* **2013**, *110*, 216801.
- [8] J. Sánchez-Barriga, A. Varykhalov, J. Braun, S. Y. Xu, N. Alidoust, O. Kornilov, J. Minár, K. Hummer, G. Springholz, G. Bauer, R. Schumann, L. V. Yashina, H. Ebert, M. Z. Hasan, O. Rader, *Phys. Rev. X* **2014**, *4*, 011046.
- [9] S. N. P. Wissing, C. Eibl, A. Zumbülte, A. B. Schmidt, J. Braun, J. Minár, H. Ebert, M. Donath, *New J. Phys.* **2013**, *15*, 105001.
- [10] Y. Xu, Z. Gan, S. C. Zhang, *Phys. Rev. Lett.* **2014**, *112*, 226801.
- [11] J. Braun, K. Miyamoto, A. Kimura, T. Okuda, M. Donath, H. Ebert, J. Minár, *New J. Phys.* **2014**, *16*, 015005.
- [12] J. Sánchez-Barriga, A. Varykhalov, J. Braun, S. Y. Xu, N. Alidoust, O. Kornilov, J. Minár, K. Hummer, G. Springholz, G. Bauer, R. Schumann, L. V. Yashina, H. Ebert, M. Z. Hasan, O. Rader, *Phys. Rev. X* **2014**, *4*, 011046.
- [13] C. Seibel, H. Maaß, H. Bentmann, J. Braun, J. Minár, K. Sakamoto, K. Shimada, H. Ebert, F. Reinert, *J. Electron Spectrosc. Relat. Phenom.* **2015**, *201*, 110.
- [14] C. Seibel, H. Bentmann, J. Braun, J. Minár, H. Maaß, K. Sakamoto, M. Arita, K. Shimada, H. Ebert, F. Reinert, *Phys. Rev. Lett.* **2015**, *114*, 066802.
- [15] Y. Kim, C. L. Kane, E. J. Mele, A. M. Rappe, *Phys. Rev. Lett.* **2015**, *115*, 086802.
- [16] C. Cacho, A. Crepaldi, M. Battiato, J. Braun, F. Cilento, M. Zacchigna, M. C. Richter, O. Heckmann, E. Springate, Y. Liu, S. S. Dhesi, H. Berger, P. Bugnon, K. Held, M. Gironi, H. Ebert, K. Hricovini, J. Minár, F. Parmigiani, *Phys. Rev. Lett.* **2015**, *114*, 097401.
- [17] Y. Wang, P. Deorani, K. Banerjee, N. Koirala, M. Brahlek, S. Oh, H. Yang, *Phys. Rev. Lett.* **2015**, *114*, 257202.
- [18] J. Liao, Y. Ou, X. Feng, S. Yang, C. Lin, W. Yang, K. Wu, K. He, X. Ma, Q. K. Xue, Y. Li, *Phys. Rev. Lett.* **2015**, *114*, 216601.
- [19] J. Sánchez-Barriga, A. Varykhalov, G. Springholz, H. Steiner, R. Kirchschrager, G. Bauer, O. Caha, E. Schierle, E. Weschke, A. A. Ünal, S. Valencia, M. Dunst, J. Braun, H. Ebert, J. Minár, E. Golias, L. V. Yashina, A. Ney, V. Hol, O. Rader, *Nat. Commun.* **2016**, *7*, 10559.
- [20] J. Sánchez-Barriga, E. Golias, A. Varykhalov, J. Braun, L. V. Yashina, R. Schumann, J. Minár, H. Ebert, O. Kornilov, O. Rader, *Phys. Rev. B* **2016**, *93*, 155426.
- [21] C. Seibel, J. Braun, H. Maaß, H. Bentmann, J. Minár, T. V. Kuznetsova, K. A. Kokh, O. E. Tereshchenko, T. Okuda, H. Ebert, F. Reinert, *Phys. Rev. B* **2016**, *93*, 245150.
- [22] J. Sánchez-Barriga, M. Battiato, M. Krivenkov, E. Golias, A. Varykhalov, A. Romualdi, L. V. Yashina, J. Minár, O. Kornilov, H. Ebert, K. Held, J. Braun, *Phys. Rev. B* **2017**, *95*, 125405.
- [23] C. Datzler, A. Zumbülte, J. Braun, T. Förster, A. B. Schmidt, J. Mi, B. Iversen, P. Hofmann, J. Minár, H. Ebert, P. Krüger, M. Rohlfing, M. Donath, *Phys. Rev. B* **2017**, *95*, 115401.
- [24] J. Krempasky, S. Muff, M. Fanciulli, H. Volfova, A. P. Weber, N. Pilet, P. Warnicke, H. Ebert, J. Braun, F. Bertran, V. V. Volobuev, J. Minár, G. Springholz, J. H. Dil, V. N. Strocov, *Nat. Commun.* **2016**, *7*, 13071.
- [25] M. Fanciulli, H. Volfová, S. Muff, J. Braun, H. Ebert, J. Minár, U. Heinzmann, J. H. Dil, *Phys. Rev. Lett.* **2017**, *118*, 067402.
- [26] J. Braun, J. Minar, H. Ebert, *Phys. Rep.* **2018**, *740*, 1.
- [27] S. V. Halilov, H. Gollisch, E. Tamura, R. Feder, *J. Phys.: Condens. Matter* **1993**, *5*, 4711.
- [28] H. Ebert, D. Ködderitzsch, J. Minár, *Rep. Prog. Phys.* **2011**, *74*, 096501.
- [29] J. Braun, *Rep. Prog. Phys.* **1996**, *59*, 1267.
- [30] G. Malmström, J. Rundgren, *Comput. Phys. Commun.* **1980**, *19*, 263.
- [31] S. H. Vosko, L. Wilk, M. Nusair, *Can. J. Phys.* **1980**, *58*, 1200.
- [32] H. Ebert et al., The Munich SPR-KKR Package, version 8.4, <http://olymp.cup.uni-muenchen.de/ak/eibert/SPRKKR> (accessed: 2020).
- [33] A. Eyers, F. Schäfers, G. Schönhense, U. Heinzmann, H. P. Oepen, K. Hünlich, J. Kirschner, G. Borstel, *Phys. Rev. Lett.* **1984**, *52*, 1559.
- [34] A. Eyers, G. Schönhense, U. Friess, F. Schäfers, U. Heinzmann, *Surf. Sci.* **1985**, *162*, 96.
- [35] G. Schönhense, A. Eyers, U. Friess, F. Schäfers, U. Heinzmann, *Phys. Rev. Lett.* **1985**, *54*, 547.
- [36] R. Feder, *Polarized Electrons in Surface Physics*, World Scientific, Singapore **1985**, p. 125.
- [37] E. Tamura, W. Piepke, R. Feder, *Phys. Rev. Lett.* **1987**, *59*, 934.
- [38] B. Schmiedeskamp, B. Vogt, U. Heinzmann, *Phys. Rev. Lett.* **1988**, *60*, 651.
- [39] N. Irmer, R. David, B. Schmiedeskamp, U. Heinzmann, *Phys. Rev. B* **1992**, *45*, 3849.
- [40] J. Henk, R. Feder, *Europhys. Lett.* **1994**, *28*, 609.
- [41] J. Henk, T. Scheunemann, R. Feder, *J. Phys.: Condens. Matter* **1997**, *9*, 2963.
- [42] M. Ärrälä, J. Nieminen, J. Braun, H. Ebert, M. Lindroos, *Phys. Rev. B* **2013**, *88*, 195413.
- [43] A. Varykhalov, D. Marchenko, M. R. Scholz, E. D. L. Rienks, T. K. Kim, G. Bihlmayer, J. Sánchez-Barriga, O. Rader, *Phys. Rev. Lett.* **2012**, *108*, 066804.
- [44] U. Heinzmann, J. H. Dil, *J. Phys.: Condens. Matter* **2012**, *24*, 173001.
- [45] S. Tognolini, S. Achilli, L. Longetti, E. Fava, C. Mariani, M. I. Trioni, S. Pagliara, *Phys. Rev. Lett.* **2015**, *115*, 046801.
- [46] R. Arafune, N. Takagi, H. Ishida, *Prog. Surf. Sci.* **2018**, *93*, 177.
- [47] A. Dal Corso, *Surf. Sci.* **2015**, *637–638*, 106.
- [48] A. Nuber, J. Braun, F. Forster, J. Minár, F. Reinert, H. Ebert, *Phys. Rev. B* **2011**, *83*, 165401.
- [49] A. Bendounan, J. Braun, J. Minár, S. Bornemann, R. Fasel, O. Gröning, Y. Fagot-Revurat, B. Kierren, D. Malterre, F. Sirotti, H. Ebert, *Phys. Rev. B* **2012**, *85*, 245403.
- [50] I. Kinoshita, T. Anazawa, Y. Matsumoto, *Chem. Phys. Lett.* **1996**, *259*, 445.
- [51] E. V. Chulkov, V. M. Silkin, P. Echenique, *Surf. Sci.* **1999**, *437*, 330.
- [52] F. Ciccacci, S. De Rossi, A. Taglia, S. Crampin, *J. Phys.: Condens. Matter* **1994**, *6*, 7227.
- [53] A. Tamai, W. Meevasana, P. D. C. King, C. W. Nicholson, A. de la Torre, E. Rozbicki, F. Baumberger, *Phys. Rev. B* **2013**, *87*, 075113.
- [54] H. Ishida, *Phys. Rev. B* **2014**, *90*, 235422.
- [55] K. Yaji, A. Harasawa, K. Kuroda, R. Li, B. Yan, F. Komori, S. Shin, *Phys. Rev. B* **2018**, *98*, 041404R.